Journal of Magnetic Resonance 208 (2011) 20–26

Contents lists available at ScienceDirect

Journal of Magnetic Resonance

journal homepage: www.elsevier.com/locate/jmr

Characterization of a 3D MEMS fabricated micro-solenoid at 9.4 T

M. Mohmmadzadeh [a,*], N. Baxan [a], V. Badilita [b,*], K. Kratt [b], H. Weber [a], J.G. Korvink [c,d], U. Wallrabe [b,d], J. Hennig [a], D. von Elverfeldt [a]

[a] Medical Physics, Department of Radiology, University Hospital Freiburg, Germany
[b] Laboratory for Microactuators, Department of Microsystems Engineering (IMTEK), University of Freiburg, Germany
[c] Laboratory for Simulation, Department for Microsystems Engineering (IMTEK), University of Freiburg, Germany
[d] Freiburg Institute for Advanced Studies (FRIAS), University of Freiburg, Germany

ARTICLE INFO

Article history:
Received 16 June 2010
Revised 25 September 2010
Available online 10 November 2010

Keywords:
Micro-solenoidal coil
B_0 mapping
B_{1unit} mapping
SNR mapping
MR microscopy

ABSTRACT

We present for the first time a complete characterization of a micro-solenoid for high resolution MR imaging of mass- and volume-limited samples based on three-dimensional B_0, B_1 per unit current (B_{1unit}) and *SNR* maps. The micro-solenoids are fabricated using a fully micro-electromechanical systems (MEMS) compatible process in conjunction with an automatic wire-bonder. We present 15 μm isotropic resolution 3D B_0 maps performed using the phase difference method. The resulting B_0 variation in the range of [−0.07 ppm to −0.157 ppm] around the coil center, compares favorably with the 0.5 ppm limit accepted for MR microscopy. 3D B_{1unit} maps of 40 μm isotropic voxel size were acquired according to the extended multi flip angle (ExMFA) method. The results demonstrate that the characterized microcoil provides a high and uniform sensitivity distribution around its center (B_{1unit} = 3.4 mT/A ± 3.86%) which is in agreement with the corresponding 1D theoretical data computed along the coil axis. The 3D *SNR* maps reveal a rather uniform signal distribution around the coil center with a mean value of 53.69 ± 19%, in good agreement with the analytical 1D data along coil axis in the axial slice. Finally, we prove the microcoil capabilities for MR microscopy by imaging *Eremosphaera viridis* cells with 18 μm isotropic resolution.

1. Introduction

There is a growing interest to extend the resolution of conventional MR systems from millimeter to micrometer range in order to resolve the structure of small samples as for instance cellular networks or even single cells. Micro RF coils generally produce high *SNR* and can provide either higher spatial resolution of mass or volume-limited samples or better temporal resolution [1,2].

Microcoil performance is usually optimized starting already in the manufacturing process where the geometrical characteristics of the coil together with the susceptibility matching of the electronics, sample and ambient (e.g. air) are important issues to be taken into account. Regarding MRI applications, coils are generally evaluated using remarkable parameters like B_0 homogeneity [3], B_1 uniformity [4], RF power efficiency [5], and *SNR* of their sensitive volume [1]. In this context, even if there are some reports focused on the characterization of solenoidal micro-coils for NMR/MRI [6–8], a complete investigation taking into account 3D B_0, B_1 per unit current (B_{1unit}) and *SNR* maps is still lacking.

The earliest developments performed for enhancing the sensitivity and resolution in MR microscopy started with the work of Aguayo et al. [9] who reported for the first time a single cell MR image using a 5 mm diameter solenoidal coil at 9.5 T with 20 G/cm gradient. Images of 10 × 13 μm in-plane resolution and 250 μm slice thickness were acquired. This work had a great impact on the recent progress that has been made for improving the micro-solenoidal coils design and performances in reaching micron-scale resolution. Consequently, several papers separately address the issue of *SNR*, B_{1unit} and B_0 mapping for characterizing micro-solenoidal coils.

Peck et al. [10] performed a very detailed investigation of the *SNR* of solenoidal micro-coils (diameters between 50 μm to 1.8 mm) with respect to their geometrical characteristics: diameter, coil length, pitch between the windings, and wire diameter.

Some papers separately address the issue of B_0, B_{1unit} and *SNR* mapping of solenoidal coils. Purea et al. [11] simulated the 2D B_{1unit} maps of a shielded solenoidal coil of 1 mm diameter operated at 750 MHz. The solenoid B_{1unit} dependency versus the coil pitch (distance between the coil loops) along the coil axis was also reported by Bentum et al. [5]. Their simulations are performed using Biot–Savart's law. Fateh [12] optimized the geometry of micro-solenoid versus its B_1 field homogeneity using simulations performed with

* Corresponding authors. Addresses: Department of Radiology, University Hospital Freiburg, Breisacher St. 60a, 79106 Freiburg, Germany. Fax: +49 761 2709379 (M. Mohmmadzadeh). Laboratory for Microactuators, Department of Microsystems Engineering (IMTEK), University of Freiburg, Georges-Köhler-Allee 102, D-79110 Freiburg, Germany. Fax: +49 (0) 761 203 7439 (V. Badilita).
E-mail addresses: mohmmad.mohammadzadeh@uniklinik-freiburg.de (M. Mohmmadzadeh), vlad.badilita@imtek.de (V. Badilita).

1090-7807/$ - see front matter © 2010 Published by Elsevier Inc.
doi:10.1016/j.jmr.2010.09.021

ANSIS software. Likewise, Seeber et al. [13] investigated the variation of FID amplitude (which is proportional to the *SNR*) versus the coil wire material and the length of the wire connecting the coil to the matching circuit. Microcoil arrays operating as field sensors were characterized by Sipilae et al. [14] based on B_0 mapping using the phase difference method. Additionally, there are only few papers addressing the capabilities of micro-solenoids in what concerns MR imaging of small samples as for instance cells [15,16] or human hair [17].

In this study we present for the first time measurement results of the 3D B_0, B_{1unit}, and *SNR* maps for a complete characterization of a 3D solenoidal microcoil with 1 mm outer diameter and 800 μm inner diameter realized in a fully compatible micro-electromechanical systems (MEMS) process by combining the advantages offered by an automatic wire-bonder with classical planar technology. Theoretical results generated according to analytical equations verify the experimental data.

2. Materials and methods

2.1. Microcoil and MR image setup

The fabrication details of the 3D solenoidal microcoil tested throughout this paper have been reported in detail in [18]. Briefly, the microcoil has been fabricated using traditional MEMS processes and an automatic wire-bonder. A CrAu layer (50/500 nm) has been patterned on a Pyrex substrate by UV photolithography and wet etching to define the pads for microcoil winding. In a second photolithographic step, SU-8 cylinders have been defined to serve both as support for the subsequent microcoil winding step and as sample holders for MR experiments. Finally the microcoil is wound around the SU-8 cylinder with great geometrical flexibility in terms of number of windings, pitch between the windings, using 25 μm diameter insulated Au wire [19]. In particular, the microcoil characterized in this work (Fig. 1a) has five windings and pitch between the windings of 50 μm, is 650 μm high, has an outer diameter of 1 mm and wall thickness of 100 μm.

The electrical parameters were measured with an *Agilent 4294A* impedance analyzer. To avoid any movement of the coils, which would be reflected in modulations of the impedance, the analyzer was connected to a *Cascade Microtech Summit 9000* probe station. The calibration of the equipment was done with measurements of an open-circuit, a short-circuit, and a precise 50 Ω resistance. The lateral distance of the measurement tips was well-defined and was included in the calibration process. The resistance of the mentioned coil was 2.5 Ω, the inductance 40 nH. This leads to a quality factor of 40 at 400 MHz.

The microcoil was operated in transmit–receive (i.e. transceive) mode. The microcoil was matched at 50 Ω and tuned to 400 MHz (Fig. 1b) by mounting it on a PCB board with tuning and matching capacitors (Fig. 1c). The measurement was done with an *Agilent E5071C* network analyzer. We achieved an S_{11} of −44 dB (Fig. 1c). The coil was connected to the MR scanner via two RG 232 and RG 174 coaxial cables with a total length of 4.5 m.

All characterization experiments were performed using a phantom sample consisting of water doped with $CuSO_4$: 4 mMol, and NaCl: 61 mMol. The T_1 and T_2 values measured for this sample at 9.4 T are 250 ms and 200 ms respectively.

MRI experiments were performed on a 9.4 T Bruker BioSpec 94/20 system (Bruker BioSpin, Ettlingen, Germany) equipped with a B-GA12S1 gradient system (max. gradient amplitude: 675 mT/m, slew rate: 4673 T/m/s). In transmission mode, the typical power consumption of a microcoil is in the order of μW. In order to decrease the RF transmission noise and increase the steering linearity of the RF at the coil input, the transmitter amplifier was bypassed and the coil directly connected to the signal generation unit (SGU). To produce the desired spin flip angles, RF power at the coil input was adjusted by setting up the attenuator level in SGU (Fig. 1d).

In order to produce the desired spin flip angles through the pulse sequences, a reference RF pulse for a determined flip angle must be determined. To adjust the 90° RF pulse, the "single pulse" routine was applied and the attenuator level in SGU was varied for a rectangular RF pulse with 1 ms duration to maximize the free induction decay (FID) signal. This attenuation level was assigned as a reference of the RF power level for the 90° RF pulse. During

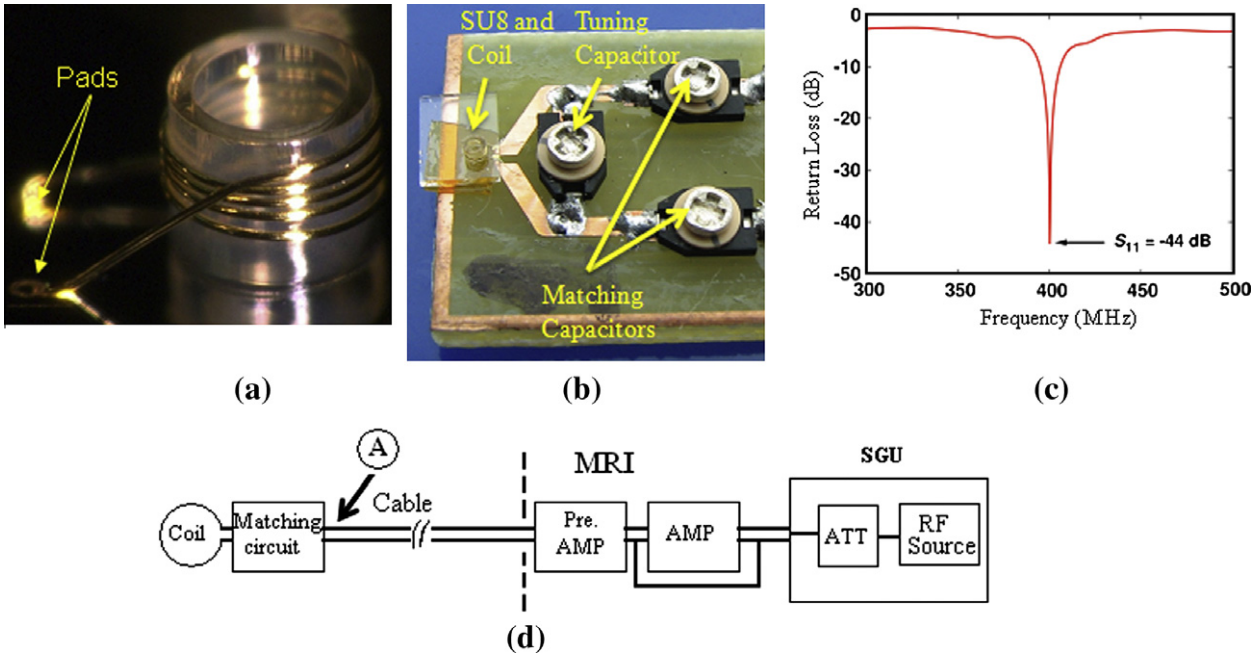

Fig. 1. (a) Image of the microcoil of 1 mm outer diameter. (b) Coil mounted on a PCB with tuning and matching capacitors. (c) Coil matching and tuning curve. (d) Coil test setup. Fig. 1d represents the coil circuit and input parts of the scanner (part MRI). The amplifier of the scanner was bypassed during the coil test.

the experiments, this value was used as a reference in the B_0, B_{1unit} and *SNR* mapping routines for producing the required spin flip angles.

2.2. B_0 mapping

The phase difference method is a well known method to measure the B_0 or Larmor frequency deviation. It can be implemented using two GE images with suitable echo time difference according to [20]:

$$\Delta\omega_0 = \gamma \cdot \Delta B_0 = \frac{\Delta\phi}{\Delta TE}. \tag{1}$$

where $\Delta\omega_0$ is the frequency deviation, γ is the gyromagnetic ratio of the hydrogen, ΔB_0 is the static magnetic field variation, $\Delta\phi$ is the phase difference, and ΔTE is the difference between two echo times.

The B_0 deviation maps were acquired inside the coil using two GE images (TR = 300 ms, ΔTE = 9.6 ms, resolution = 15 μm isotropic, measurement time = 40 min: 56). All procedures including phase subtraction, phase unwrapping, $\Delta\omega_0$ calculation, and the resulted maps were performed in Matlab (The MathWorks, Inc., Natick, MA).

2.3. B_{1unit} mapping

To measure B_{1unit} the extended multi flip angle (Ex MFA) method was performed by acquiring 10 series of 3D GE images (TR/TE = 1250/5.06 ms, resolution = 40 μm isotropic, rectangular RF pulse, τ = 0.5 ms, measurement time = 7 h: 6) by varying the spin flip angles. For this purpose, output power of SGU was changed consecutively to generate flip angles from 10° to 400° with 39° steps to cover a full period of a sine wave. Then GE images were acquired for each flip angle to produce a data course for each image voxel. B_{1unit} profile was produced by fitting an appropriate sine wave for each voxel data in Matlab using the following equations [21]:

$$S(I) = \kappa\sqrt{S_x(I)^2 + S_y(I)^2} \tag{2}$$

with

$$S_x(I) = \sin(\theta(I)) \cdot \sin(\alpha(I)), \tag{2a}$$

$$S_y(I) = \cos(\theta(I)) \cdot \sin(\theta(I)) \cdot (1 - \cos(\alpha(I))), \tag{2b}$$

where $S(I)$ is the voxel signal for the coil current I, $S_x(I)$ and $S_y(I)$ are the x and y components of $S(I)$ and the proportionality constant κ incorporates the remaining constant terms. The coil-current dependent flip angle $\alpha(I)$ is described by:

$$\alpha(I) = \tau\sqrt{(\Delta\omega 2\pi)^2 + (B_{1unit} I\gamma)^2} \tag{3}$$

with γ the gyromagnetic ratio, $\Delta\omega$ the off-resonance frequency during excitation and τ the RF pulse duration which was 0.5 ms for all images. The angle $\theta(I)$ describes the off-resonant dependent orientation between B_0 and the effective excitation field:

$$\theta(I) = \frac{\pi}{2} - \tan^{-1}\left(\frac{\Delta\omega 2\pi}{B_{1unit} I\gamma}\right) \tag{4}$$

According to Eqs. (2), (2a), (2b), (3), (4), for finding the fitting curve, the coil current value needs to be determined for each $S(I)$. For this purpose, at first we measured the non attenuated RF power P_0 at the coil input (point A in Fig. 1d) by adjusting 0 dB attenuation in SGU unit. It was measured using a spectrum analyzer (*Agilent 4396B*) after applying the single pulse routine and setting the attenuation level in SGU to 0 dB. Its measured value was 0.588 mW.

Next, the coil current I_i was computed for each image based on the adjusted attenuation in SGU according to [22] as follows:

$$I_i = \sqrt{\frac{P_0 - P_i}{R_{coil}}} \tag{5}$$

where P_i is the power attenuation level in SGU, R_{coil} is the real part of coil impedance (2.5 Ω measured value at 400 MHz).

As a reference for confirming the accuracy of the experimental B_{1unit} maps, 1D B_{1unit} variation along the coil axis was calculated according to Biot–Savart law using [23]:

$$B_{1unit} = \frac{B_1}{i} = k\frac{\mu_0 \cdot n}{2l}\left[\frac{x + l/2}{\sqrt{a^2 + (x + l/2)^2}} - \frac{x - l/2}{\sqrt{a^2 + (x - l/2)^2}}\right] \tag{6}$$

where the origin of x is defined at the center of the coil, k equal to 0.5 represents the right-handed rotating component of the magnetic field (measured B_{1unit}) and it is half of the value given by the Bio–Savart law [24], μ_0 is the permeability of free space, n is the number of turns, a and l are the radius and length of the solenoid respectively. At the coil center (x = 0) formula (6) reduces to:

$$B_{1unit} = \frac{B_1}{i} = k\frac{\mu_0 \cdot n}{2a}\left[\frac{1}{\sqrt{1 + (l/2a)^2}}\right] \tag{7}$$

2.4. Image SNR

The quality of the obtained images is evaluated by mapping the *SNR* of the sensitive volume of the microcoil per each voxel. According to Hoult and Richard the voxel *SNR* is proportional to [25]:

$$SNR \propto \frac{B_{1unit}}{\sqrt{R_{noise}}} \tag{8}$$

where B_{1unit} is the magnetic field induced in the coil per unit current and R_{noise} represents the conductive losses of the coil, circuit and sample.

To measure the coil *SNR* per voxel two separate spin echo images were acquired according to the method described in Ref. [26]. The first image was an SE image (TR/TE = 500/16.3 ms, resolution = 15 μm isotropic, transmitter attenuation level = 15 dB, measurement time = 9 h: 6) to derive the voxel signal. The second one (TR/TE = 60/16 ms, resolution = 15 μm isotropic, transmitter attenuation level = 150 dB, measurement time = 8 min: 5) was acquired to compute the noise value. The noise and signal sequences had the same parameters except for the TR and RF power attenuation parameters which were set to 60 ms and 150 dB for the noise sequence. As the sample was uniform, the standard deviation of the signal distribution of the noise image at the sample location was assigned as noise value for all voxels. The image *SNR* was further determined by dividing the voxel signal to the noise.

2.5. Cell image

To evaluate the coil performance on single cell MRI, MR images of algae cells (*Eremosphaera viridis*) of 100–120 μm diameter were acquired using a 3D spin-echo sequence (TR/TE = 600/16 ms, resolution = 18 μm isotropic, measurement time = 10 h: 44). The cells were loaded inside the SU-8 capillary by dispersing them in doped water into the sample container with a pipette. Next, the sample container was directly closed with an adhesive film (ABgene, Fisher Sci GmbH) in order to prevent evaporation thus enabling long high resolution scans with minimum artifacts due to movement.

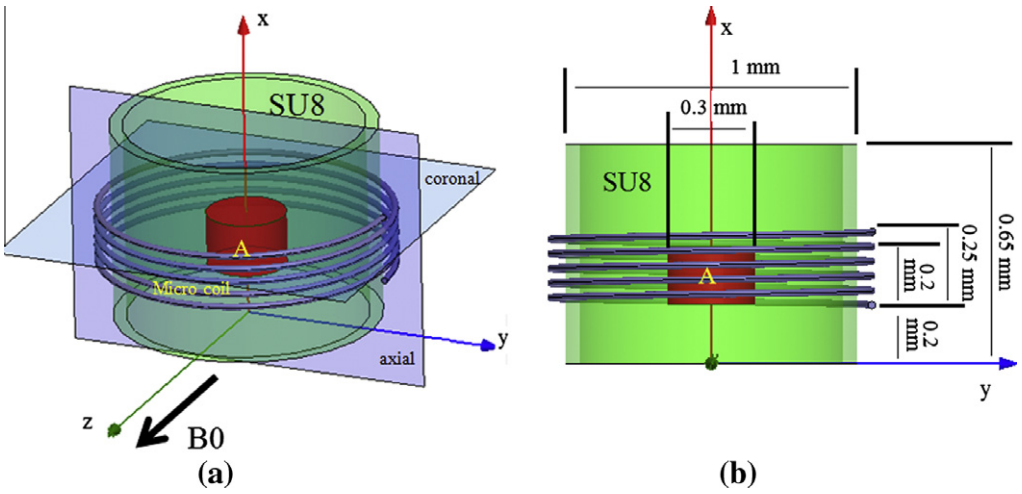

Fig. 2. (a) 3D view of the orientation of the microcoil, sample and slice selection, in the MR setup and (b) 2D view of the microcoil and its geometry. In Fig. 2a, the coronal slice is in parallel to B_0 and the axial one is perpendicular to it. Quantitative data of B_0, B_1unit, and *SNR* are generated from volume A.

Table 1
Mean and relative standard deviation of ΔB_0, B_{1unit}, and *SNR* values in the region A (Fig. 2).

	ΔB_0		B_{1unit} (mT/A)	*SNR*
	Hz	ppm		
Mean	−46.23	−0.11	3.4	53.89
Relative STD %	36		3.8	19

3. Results

The MR setup including the microcoil positioning relative to B_0 and the slice selection is illustrated in Fig. 2. Volume A shows a region around the coil center with lower ΔB_0 and more uniform B_{1unit} and *SNR* distributions. The radius and height of the cylindrical region A are 150 μm and 200 μm respectively. Quantitative data of B_0, B_1unit, and *SNR* are generated from this volume, and are summarized in Table 1. Fig. 3[1] shows the B_0 mapping of the solenoid coil in coronal and axial slices. From the displayed color bars it can be noticed that the absolute value of the B_0 deviation reaches a maximum of 250 Hz corresponding to 0.62 ppm. The mean and relative standard deviation (STD)/mean; STD; of ΔB_0 computed from the volume marked as A (see Fig. 2a) is given in Table 1. The values displayed here are given both in Hz and ppm for comparing them with the accepted limit in MR microscopy which is generally evaluated in ppm [11].

Fig. 4a and b shows the B_{1unit} maps in the coronal and axial slices of the micro-solenoidal coil. The mean and relative STD values of B_{1unit} computed within volume A (see Fig. 2) are indicated in Table 1. As it is illustrated in Fig. 4, the B_{1unit} profile is not uniform through the whole sample increasing at the proximity of the coil wires.

Fig. 4c represents the theoretical calculation and the experimental B_{1unit} variation along the coil axis (Line A in Fig. 4b). According to Eq. (7) and the geometrical characteristics of the micro-solenoid, the B_{1unit} value at the coil center was 3 mT/A which is in close agreement to the measured value of 3.5 mT/A.

Fig. 5 shows the *SNR* maps of the micro-solenoidal coil in coronal and axial slices. The mean and relative STD values of the *SNR* distribution in the region A (see Fig. 2) is given in Table 1. Additionally, the mean value of *SNR* throughout the whole sample was obtained 72.6 ± 45% per 3.4 pl voxel size.

The experimental results were compared to the simulated ones according to Eq. (8). The *SNR* profile was measured along line L1 (as shown in Fig. 5b) and displayed together with the analytical curve in Fig. 5c. The obtained values were normalized to the related maximum values.

The feasibility of taking MR images of cells with such micro-devices is illustrated in Fig. 6a. The measured cells diameter was found between 100 and 125 μm. Moreover, delineation of structures inside the cell was possible as well, the MR images being compared with photos taken from microscope (Fig. 6b). The measured contrast to noise ratio between doped water and cells was 1.7.

4. Discussion

We characterized a MEMS micro-solenoidal coil of 1 mm diameter with respect to the 3D maps of B_0, B_{1unit}, and *SNR* using the previously described methods. Although these techniques are already standard methods for characterizing conventional large MR coils, their application on solenoidal micro-coils was reported only on few papers.

The fabrication techniques used in this paper combine the advantages given by the MEMS technology with those offered by the automatic wire bonding procedure. More specifically, MEMS processing and materials (SU-8 in this case) potentially enable further microfluidic integration for automatic probe handling and delivery. In addition, inner and outer diameters of the microcoil are determined with the resolution given by the photolithographic process. This provides the freedom to fabricate reproducible micro-coils with smaller diameters and desired SU-8 sidewalls in order to get higher B_{1unit} values and less B_0 deviation on the coil sensitive volume in MR microscopy. One limitation of the current technology is the use of Au wire, which introduces a rather high susceptibility mismatch with respect to the surrounding materials increasing the B_0 deviation through the sample. Replacing the Au with Cu wire would be the next step to significantly improve the performance of these micro-coils.

In this study we could not compare the performance of the MEMS micro-coil with other coils of the same geometry, fabricated by other techniques like manually or custom made machine ones. The main reasons are: (1) it was not possible to manually wind the Au wire around the micro-fragile SU-8 cylinder and (2) there was no available paper on the characterization of the manually wounded

[1] For interpretation of color in Fig. 3, the reader is referred to the web version of this article.

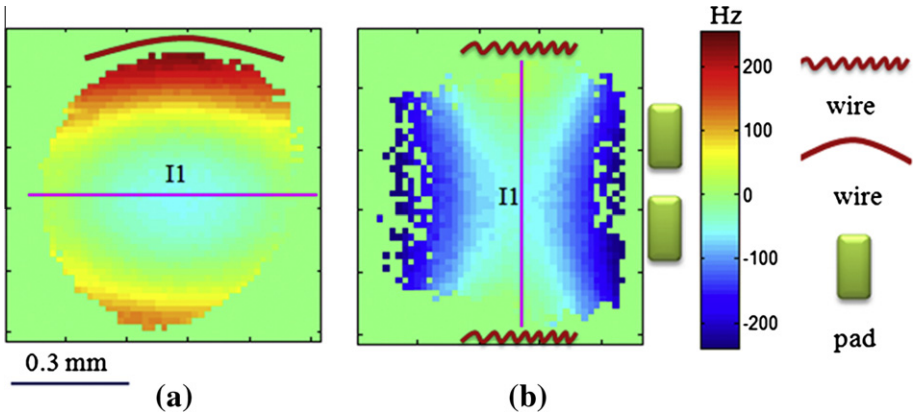

Fig. 3. B_0 mapping of the sensitive microcoil volume displayed in: (a) coronal slice and (b) axial slice (see Fig. 2a) which are positioned at the coil center. Lines I1 show the intersection of the coronal and axial plane. To show the coil orientation in the 2D maps, the position of the coil wires and pads are represented in this figure.

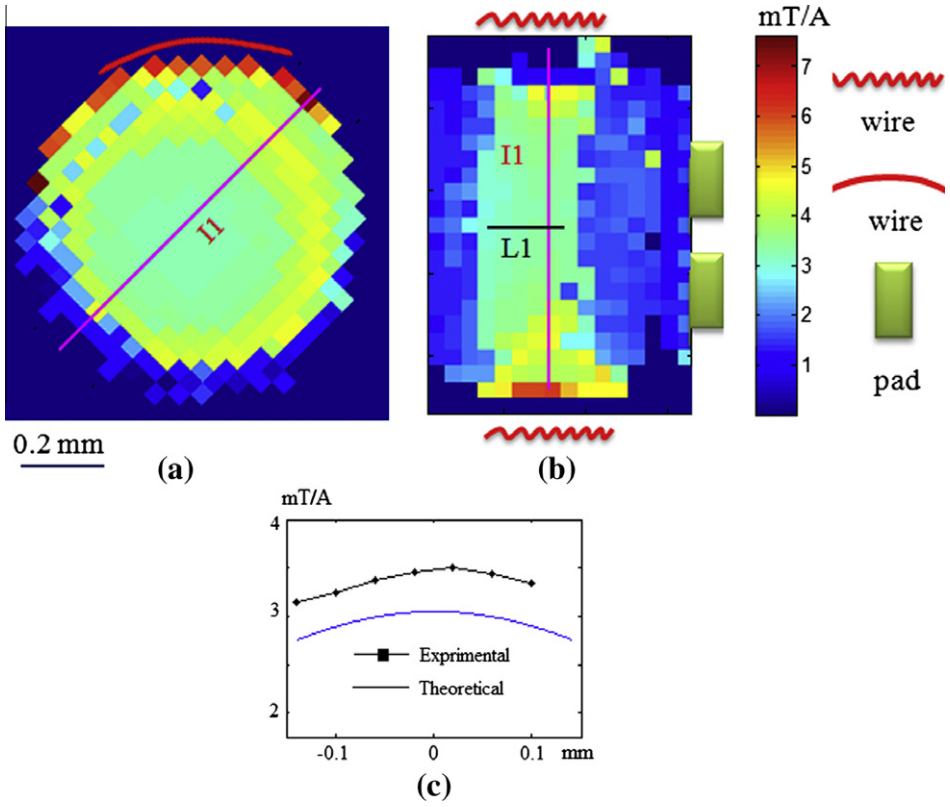

Fig. 4. B_{1unit} maps displayed in: (a) coronal slice and (b) axial slice (see Fig. 2a) and (c) theoretical and measured values of the B_{1unit} along the line L1 (see Fig. 4b). Line I1 in Fig. 4a represents the intersection of the coronal and axial planes. The location of coil wire and pads was added for illustrating the coil orientation. In Fig. 4c the curve marked with dots shows the experimental curve.

or lithographic solenoidal micro-coils [27] having the same geometry as our coil. Therefore, the acquired results have been evaluated with the existing reference in B_0 mapping [11] and with the results of analytical equations in B_{1unit} and *SNR* mapping.

As the color bar in Fig. 3 indicates it, the maximum B_0 deviation in coronal and axial slices was ± 250 Hz (or ± 0.62 ppm) while around the coil center (region A in Fig. 2) according to Table 1, it has decreased to −46.2 Hz (−0.11 ppm) ± 36%. Close to the pads the B_0 deviation is increasing probably due to the susceptibility mismatch between the microcoil Au wire and the doped water sample causing a stronger variation of the B_0 field. We believe that the B_0 deviation of 0.5 ppm is still acceptable for performing MR microscopy [11]; therefore we can conclude that a large sensitive area of the microcoil is suitable for MR imaging.

Fig. 4a and b displays a relatively uniform B_{1unit} distribution inside the coil particularly in region A (see Fig. 2) with a mean value of B_{1unit} = 3.4 mT/A and with changes of only ± 3.86% (see Table 1). As expected, the sensitive profile of the microcoil is rather homogenous, making it appropriate to use it in transmission mode.

The Biot–Savart law (without the factor k) gives the amplitude of B_1 in the laboratory frame which is sum of two rotating magnetic fields: one B_{1cw}, is rotating clockwise and the other, B_{1ccw}, is rotating counterclockwise. Therefore to calculate the corresponding theoretical value of B_{1unit} (B_{1cw} per unit current) a constant factor k = 0.5 is included in Eqs. (6) and (7) [24].

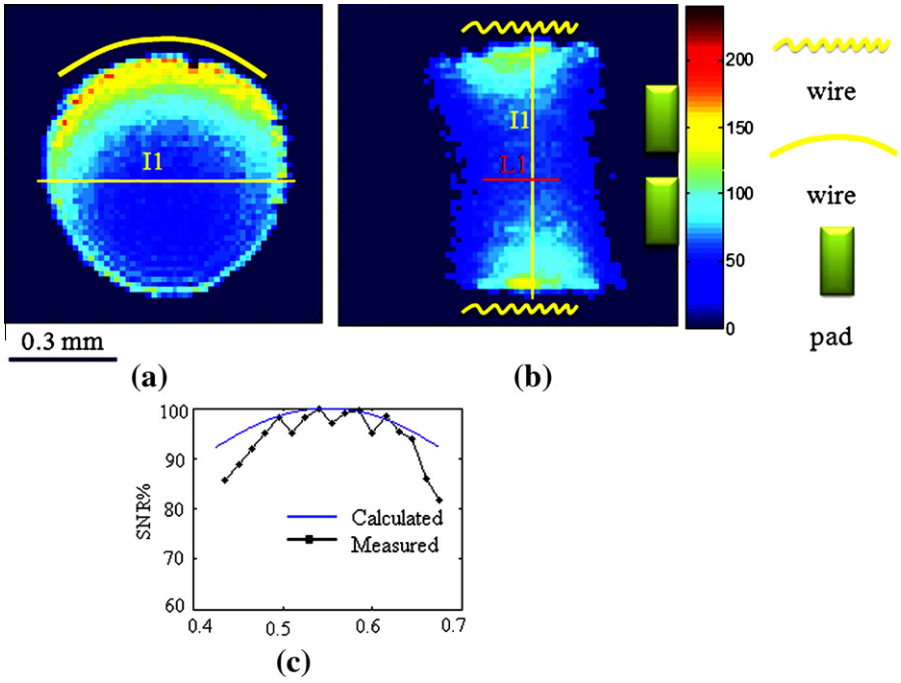

Fig. 5. *SNR* maps displayed in: (a) coronal and (b) axial slices (see Fig. 2a) and (c) the *SNR* measured along coil axis (see the line L1 in Fig. 5b). Lines I1 in Fig. 5a show the intersection of coronal and axial planes. The coil wire and pads are shown next to the computed maps for showing the coil orientation. The curve marked with dots shows the experimental curve.

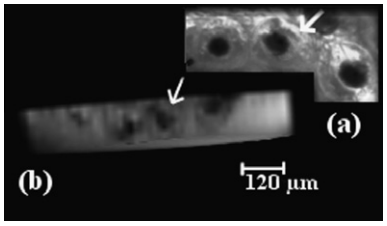

Fig. 6. (a) Microscope picture of the sample image in (b). The sample consists of three algae cells, *Eremosphaera viridis*, with diameters ranging from 100 to 120 μm. The white arrows illustrate one single cell as it was observed on microscopy and MRI respectively.

As indicated in Fig. 4c, experimental and theoretical B_{1unit} curves along the coil axis are in good agreement. At the coil center the measured B_{1unit} value is 3.5 mT/A and the theoretic value is 3 mT/A.

3D B_{1unit} maps show that the B_{1unit} distribution is not uniform through the slices and it increases at the proximity of coil wires. This enhancement is in part related to a higher ΔB_0 value at the windings proximity. According to Fig. 3, the B_0 deviation might still affect the image intensity in this area even if its influence has been considered in the B_{1unit} data calculation (Eqs. (3) and (4)).

Fig. 5a and b illustrates a relatively uniform area for the *SNR* distribution in the large area of the coronal and axial slices. Moreover Table 1 indicates that the microcoil provides a relatively high *SNR* in the region A (see Fig. 2) with the value of 53.69 ± 19% for such a small voxel size of only 15 pL which is promising for performing MR microscopy. In addition, the mean of the measured *SNR* value through the whole sample is higher than the mean *SNR* value of the volume A which is 74 ± 45%. We notice as well a similar signal enhancement pattern as in the B_{1unit} maps in areas located near the pads and coil wires. Consequently, based on the results obtained from the B_{1unit}, B_0 maps and Eq. (8) we can conclude that, even if the high intensity areas in *SNR* maps are produced due to higher B_{1unit} value, there is still an influence of the B_0 deviation effects mostly near the coil wires and pads in 2D B_{1unit} and mainly *SNR* maps. In Fig. 5a, the high intensity area is asymmetrically distributed while in Fig. 5b a more symmetrical pattern is obtained. This is a well known effect of solenoids which originates in the helical winding of the coil and will occur even if the measurement plane is perfectly perpendicular to the microcoil axis. The experimental *SNR* distribution was found in good agreement with the corresponding theoretical 1D *SNR* curves along the coil axis (see line L1 in Fig. 5b). However, as the distance from the coil center increases, the differences are more severe mainly caused by the B_0 deviation effect and non uniform winding of the coil. Consequently, the comparison between theoretical and experimental data was performed only at the central region of the micro-solenoid.

As shown in Fig. 6a, high resolution MRI of single cells was possible using the 3D solenoidal microcoil. A voxelsize of 18 μm isotropic corresponds to a realistic resolution for MR microscopy applications. The micro-solenoid provides enough *SNR* to differentiate the cell geometries (diameter 105–120 μm) inside the water phantom which were readily identified in the microscope picture. However, acquisition time of several hours is required. In that case, perfusion of the cells is necessary to maintain stable environmental conditions and cell viability.

In summary, based on the B_0, B_{1unit}, and *SNR* maps distribution we do believe that MR microscopy of cells is feasible using the micro-solenoid coil. Moreover, the uniform area at the coil center extends sufficiently to enable cell handling and therefore the acquisition of highly resolved MR images with minimum B_0 and B_{1unit} artifacts becomes possible.

5. Conclusion

We have characterized a 3D MEMS fabricated micro-solenoid coil operated in transceiver mode using 3D maps of B_0, B_{1unit}, and *SNR*. All maps and the cell image demonstrate the coil performance in MR microscopy. For verifying the experimental results, the theoretical 1D curve was included in this study.

It is known that the coil characterization based on the above mentioned methods performed throughput the entire sensitive volume illustrates the coil abilities in MR imaging. For instance, the B_{1unit} field uniformity is an important index for using the coil in transmission mode [28]. Likewise the B_0 variation mainly arises from the susceptibility mismatch in and around the active region of the microcoil, mapping its value in each voxel could provide valuable information for evaluating the magnetic field inhomogeneity in the coil/sample system and its local surrounding. Moreover, the *SNR* uniformity and magnitude could primarily indicate if the coil is suited for real time imaging or *in vivo* active tracking applications.

According to the generated 3D maps and cell MR images, we conclude that the central sensitive region of the microcoil is large enough to contain and to image single cells since the B_{1unit}, and *SNR* distribution at this region is rather uniform and intense and the B_0 field deviation is minimal. The B_0 homogeneity can be further improved particularly at the pads position by matching the susceptibility of the coil, wires, SU-8, sample and environment. Secondly manufacturing smaller coils will increase the filling factor and consequently the B_{1unit} field and the *SNR*. These are important issues that have to be taken into account when designing such micro-devices and they will be highly considered for future studies.

Acknowledgment

This work was supported by the European Union (FP6-NEST-2004: Micro-MR). We hereby acknowledge financial support from the BMBF and the Excellence Initiative of the German Federal and State Governments.

References

[1] A. Webb, Radiofrequency microcoils in magnetic resonance, Prog. Nucl. Magn. Reson. Spectrosc. 31 (1997) 1–42.
[2] D.I. Hoult, The NMR receiver: a description and analysis of design, Prog. NMR Spectrosc. 12 (1978) 41–77.
[3] J.F. Schneck, The role of magnetic susceptibility in magnetic resonance imaging: MRI magnetic compatibility of the first and second kinds, Med. Phys. 23 (1996) 815–850.
[4] G.J. Barker, A. Simmons, S.R. Arridge, P.S. Tofts, A simple method for investigating the effect of non-uniformity of radiofrequency transmission and radiofrequency in MRI, Br. J. Radiol. 71 (1998) 59–67.
[5] P.J.M. Bentum, J.W.G. Janssen, A.P.M. Kentgens, Towards nuclear magnetic resonance μ-spectroscopy and μ-imaging, Analyst 129 (2004) 793–803.
[6] R. Subramanian, M.M. Lam, A.G. Webb, RF micro coil design for practical NMR of mass-limited samples, J. Magn. Reson. 133 (1998) 227–231.
[7] R. Kc, I.D. Henry, G.H.J. Park, D. Raftery, Design and construction of a versatile dual volume heteronuclear double resonance microcoil NMR probe, J. Magn. Reson. 197 (2009) 186–192.
[8] M. Mohammadzadeh, H. Weber, N. Baxan, V. Badilita, J. Maclaren, J. Hennig, D.V. Elverfeldt, B1 and B0 Mapping of a Micro Helix Coil at 9.4 T, Stockholm, ISMRM 2010, p. 3907.
[9] J.B. Aguayo, S.J. Blackband, J. Schoeniger, M.A. Mattingly, M. Hintermann, Nuclear magnetic resonance imaging of a single cell, Nature 322 (1986) 190–191.
[10] T.L. Peck, R.L. Magin, P.C. Lauterbur, Design and analysis of microcoils for NMR microscopy, J. Magn. Reson. 108 (1995) 114–124.
[11] A. Purea, T. Neuberger, A.G. Webb, Simultaneous NMR microimagimg of multiple single-cell samples, Concept Magn. Reson Eng. 22B (2004) 7–14.
[12] B. Fateh, Modeling, Simulation and Optimization of a Microcoil for MRI-Cell Imaging, Master Thesis, Freiburg University, 2006.
[13] D.A. Seeber, R.L. Ciobanu, C.H. Pennington, Design and testing of high sensitivity microreceiver coil apparatus for nuclear magnetic resonance and imaging, Rev. Sci. Instrum. 72 (4) (2001) 2171–2179.
[14] P. Sipilae, D. Lange, S. Lechner, W. Loew, P. Gross, M. Baller, G. Wachutka, F. Wiesinger, Robust, susceptibility-matched NMR probes for compensation of magnetic field imperfections in magnetic resonance imaging (MRI), Sens. Actuators 145–146 (2008) 139–146.
[15] S.C. Lee, K. Kim, J. Kim, S. Lee, J.H. Yi, S.W. Kim, K.S. Ha, C. Cheong, One micrometer resolution NMR microscopy, J. Magn. Reson. 150 (2001) 207–213.
[16] L. Ciobanu, D.A. Seeber, C.H. Pennington, 3D MR microscopy with resolution 3.7 μm 3.3 μm by 3.3 μm, J. Magn. Reson. 158 (2002) 178–182.
[17] E. Mattle, M. Weiger, D. Schmidig, P. Boesiger, M. Fey, MRI of human hair, Magn. Reson. Mater. Phys. Biol. Med. 22 (2009) 181–186.
[18] V. Badilita, K. Kratt, N. Baxan, M. Mohmmadzadeh, T. Burger, H. Weber, D.V. Elverfeldt, J. Hennig, J.G. Korvinkc, U. Wallrabe, On-chip three dimensional microcoils for MRI at the micro-scale, Lab Chip 10 (2010) 1387–1390.
[19] K. Kratt, V. Badilita, T. Burger, J.G. Korvink, U. Wallrabe, A fully MEMS-compatible process for 3D high aspect ratio micro coils obtained with an automatic wire bonder, J. Micromech. Microeng. 20 (2010) 015021 (11pp).
[20] H.-H. Chen, R.D. Boykin, G.D. Clarke, J.H. Gao, J.W. Roby, Routine testing of magnetic field homogeneity on clinical MRI systems, Med. Phys. 33 (2006) 4299–4306.
[21] H. Weber, D. Paul, D.V. Elverfeldt, J. Henning, M. Zaitsev, Extended multi-flip-angle B1 mapping: A 3D mapping method for inhomogeneous B1 fields, Concepts Magn. Reson. 37B (2010) 203–214.
[22] D.K. Cheng, Field and Wave Electromagnetics, Addison-Wesley, 1989.
[23] J. Mispelter, M. Lupu, A. Briguet, NMR Probe Heads for Biophysical and Biomedical Experiments, Imperial College Press, 2006.
[24] J. Jianmin, Electromagnetic Analysis and Design in Magnetic Resonance Imaging, CRC Press, 1998.
[25] D.I. Hoult, R.E. Richards, The signal-to-noise ratio of the nuclear magnetic experiment, J. Magn. Reson. 24 (1976) 71–85.
[26] National Manufacturers Electrical Association, MS1-2001 Determination of Signal-to-Noise Ratio (SNR) in Diagnostic Magnetic Resonance Images, Washington, 2001.
[27] V. Demas, A. Bernhardt, V. Malba, K.L. Adams, L. Evans, C. Harvey, R.S. Maxwell, J.L. Herberg, Electronic characterization of lithographically patterned microcoils for high sensitivity NMR detection, J. Magn. Reson. 200 (2009) 56–63.
[28] E.K. Insko, L. Bolinger, Mapping of the radiofrequency field, J. Magn. Reson. 103 (1993) 82–85.